JOURNAL OF GEOPHYSICAL RESEARCH, VOL. 112, C08008, doi:10.1029/2005JC003309, 2007

Determining heterogeneous bottom friction distributions using a numerical wave model

T. R. Keen,[1] W. E. Rogers,[1] J. Dykes,[1] J. M. Kaihatu,[1] and K. T. Holland[2]

Received 22 September 2005; revised 15 March 2007; accepted 1 June 2007; published 11 August 2007.

[1] This paper describes a method for estimating spatially variable bottom roughness lengths (k_b) in friction-dominated coastal regions where dense measurements of the significant wave height are available. The method utilizes a numerical wave model to calculate wavefields. The model-predicted significant wave height is compared to a control simulation with a known k_b field, which is a proxy for measured wave heights. The error is used in combination with an influence matrix to successively correct the bottom roughness field. This predictor-corrector calculation is completed in a series of analysis cycles. The method is demonstrated in an idealized basin with different k_b distributions. The test cases simulate swell propagating over a sloping beach. The original k_b fields are recovered in a reasonable number of analysis cycles but the method is limited by the influence of bottom friction on the wave height. The inversion is shown to be robust in the presence of errors in the measured wavefield as well as random bathymetry errors. However, the inversion fails if bathymetry errors are large and/or systematic because the friction error is not substantially greater than the error from bathymetry, which is also a key parameter for calculating the wave height. Thus it is important to select parameters and variables that have well-defined dependencies in the numerical wave model for this procedure to be effective.

Citation: Keen, T. R., W. E. Rogers, J. Dykes, J. M. Kaihatu, and K. T. Holland (2007), Determining heterogeneous bottom friction distributions using a numerical wave model, *J. Geophys. Res.*, *112*, C08008, doi:10.1029/2005JC003309.

1. Introduction

[2] It is not possible to completely observe the global ocean but remote sensing has made it easier to measure sea surface properties over large regions. The observation problem is even greater for the seafloor. Although bottom friction is not critical to understanding the dynamics of ocean currents in deep water, it can be important for both currents and waves in the shallow water over the continental shelf. When the water depth is less than the deep-water wavelength of wind-generated surface waves, bottom friction can produce observable changes in the surface wave properties (most obviously, dissipation of wave energy as waves propagate) as demonstrated in recent work [*Sheremet and Stone*, 2003; *Ardhuin et al.*, 2003; *Kaihatu and Sheremet*, 2004]. These changes can be observed remotely, as can other ocean surface properties like wave energy spectra and temperature. However, when only surface properties are available, it is problematic to determine the causes of the observed changes. Because of these difficulties, ocean scientists have begun to utilize inverse techniques, which can improve our knowledge of physical processes from observations.

[3] One kind of inverse method is data assimilation, which combines model physics with observations to provide a better picture of the ocean than can be deduced from either alone [*Anderson et al.*, 1996]. Data assimilation techniques range from nudging numerical models with observations to direct assimilation of observations using variational approaches [*Le Dimet and Talagrand*, 1986; *Bennett*, 1992; *Bertino et al.*, 2003]. Data assimilation has been used to improve numerical wave forecasts by nudging wave models with observations from wave buoys and remote sensing [*O'Reilly and Guza*, 1998; *Holthuijsen et al.*, 1997; *Bidlot and Holt*, 1999; *Greenslade*, 2001]. In addition to its use in improving wave forecasting, assimilation has also proven useful in estimating water depth using inverse techniques [*Dalrymple et al.*, 1998; *Grilli*, 1998; *Wackerman et al.*, 1998], and iterative approaches are necessary for depth inversions based on numerical wave modeling [*Kennedy et al.*, 2000].

[4] Data assimilation requires that some assumptions be made with respect to the relationships between the data and model parameters being investigated. Numerical wave models that include physical phenomena such as shoaling, dissipation, bottom friction and refraction can permit a comprehensive examination of complex processes. However, in order to use a numerical wave model in an inverse solution, it is necessary to first identify the key model parameters. Key model parameters are those upon which all other parameters have a high dependency. They can be identified by sensitivity analyses using a numerical model

[1] Oceanography Division, Naval Research Laboratory, Stennis Space Center, Mississippi, USA.
[2] Marine Geosciences Division, Naval Research Laboratory, Stennis Space Center, Mississippi, USA.

0148-0227/07/2005JC003309$09.00

[*Sun et al.*, 2001; *Weisse and Feser*, 2003] but it is important to test for consistency in the selection of key parameters when complex models are used [*Beck*, 1987; *Feddersen et al.*, 2004]. Water depth is one key parameter in numerical wave models for shallow water studies and a second one is the bottom roughness, which contributes to both bottom friction and dissipation.

[5] This study focuses on retrieving the bottom roughness length k_b using an inversion method based on a numerical wave model. Determining the appropriate distribution of bottom roughness for a given wavefield with a numerical wave model requires the following conditions to be met: (1) the model equations must capture the physical relationship between bottom friction and the wavefield; (2) it is necessary to have a dense set of observations; and (3) the solution must be unique for the selected key parameter. The numerical wave model must include a bottom friction dissipation term in the model equations that explicitly represents the nonlinear damping of wave energy caused by bottom roughness (condition 1). We use a numerical wave model to produce a database that represents a dense set of observations (condition 2). We will meet condition 3 by demonstrating that the inversion works for small bathymetric errors because the influence of water depth on the wavefield is distinct from that of bottom friction.

[6] This paper describes an inversion method for determining the bottom friction field in a coastal area for which the bathymetry is known. The purpose of the technique is to learn more about the bottom using the physics of energy dissipation by bottom friction. The method utilizes a numerical wave model in an iterative procedure similar to previous studies [e.g., *Kennedy et al.*, 2000; *Narayanan et al.*, 2004]. The *Kennedy et al.* [2000] approach uses observations of wave speed to make local corrections to the bathymetry. In the present study, the global impact of a modified variable on the observations is contained within an influence matrix, which permits nonlocal effects to be included in the inversion. We will demonstrate that this approach can be used if the key parameters are well defined. This study will focus on wave height because it can be measured by both in situ and remote observation methods. This inversion method is intended for use with dense data sets from remote sensing, including satellites and coastal radar systems [e.g., *Haus*, 2007]. However, no such observations were available for this study, so these data sets will be represented by a series of control runs using a numerical wave model. The inversion procedure will then attempt to reproduce these wavefields while recovering the original bottom roughness distributions.

[7] Section 2 describes the numerical wave model used in this study and the model setup for the different cases examined. Section 3 presents the inversion method and section 4 discusses the results for retrieved bottom friction fields. Section 5 examines the sensitivity of the inversion to noise and unknown errors in bathymetry and section 6 discusses some of the issues inherent in applying this approach.

2. Wave Simulations

[8] The approach described in this paper does not depend on the wave model used but it is necessary that the model contains the key parameter of interest. We use the SWAN (Simulating Waves Nearshore) model, which includes terms for refraction, reflection caused by currents and water depth, wave breaking, dissipation by bottom friction and white-capping, wave-wave interaction, and local wind generation. Recent versions of SWAN also calculate diffraction, but they were not used in this study. SWAN incorporates depth-induced breaking but it is turned off for this study. White capping, wind input, and nonlinear interactions are also turned off.

[9] The SWAN wave model represents surface waves with the two-dimensional wave action density spectrum $N(\sigma,\theta)$, where σ is the relative frequency and θ is the wave direction [*Booij et al.*, 1999]. The wave spectrum is described by the spectral action balance equation:

$$\frac{\partial N}{\partial t} + \nabla \cdot \vec{C} N = \frac{S}{\sigma} \tag{1}$$

where: ∇ = the gradient operator in x, y, θ, and σ; $\vec{C}$ = the group velocity; and the source term S is given by $S = S_{bf} + S_{other}$. For a discussion of the other source terms S_{other}, the interested reader is referred to *Booij et al.* [1999]. The bottom friction term S_{bf} is defined by:

$$S_{bf}(\sigma,\theta) = -C_{bf}\frac{\sigma^2}{g^2 \sinh^2(kd)} E_D(\sigma,\theta) \tag{2}$$

where: g = the gravity constant; k = wave number; d = water depth; and E_D = the energy density. The drag coefficient C_{bf} is given by $C_{bf} = f_w \frac{g}{\sqrt{2}} U_{rms}$ where U_{rms} is a bottom orbital velocity. The wave friction factor f_w is found by solving the following equation:

$$\frac{1}{4\sqrt{f_w}} + \log_{10}\left[\frac{1}{4\sqrt{f_w}}\right] = 0.08 + \log_{10}\left[\frac{a_b}{k_b}\right] \tag{3}$$

[10] Equation (3) contains the near-bottom excursion amplitude a_b and the bottom roughness k_b. The bottom friction formulation used in this study is the eddy viscosity model of *Madsen et al.* [1988]. Three values of the roughness length k_b are used: 0.005 m, 0.05 m, and 0.07 m. Sensitivity tests with the wave climate used herein showed that for larger values of k_b, there is an effective cap on the bottom friction term for the Madsen formula. A roughness length k_b of 0.05 m is used as the background value in all of the simulations because it is a typical value associated with ripples on the inner shelf.

[11] SWAN integrates (1) with finite difference schemes for time, geographic space, and spectral space. A curvilinear grid (Figure 1) is used for the prognostic wave calculations by SWAN and the wavefields are output on a uniformly spaced grid (hereinafter termed output grid or OG) using bilinear interpolation, which is incorporated within SWAN. The OG is representative of remotely sensed or measured wavefields. Nodes on this grid are denoted i_o and j_o along the x (easting) and y (northing) axes, respectively. A uniform output grid is more convenient for processing the wave height and wave height error fields. The use of different calculation and output grids introduces some interpolation errors, which are considered acceptable for

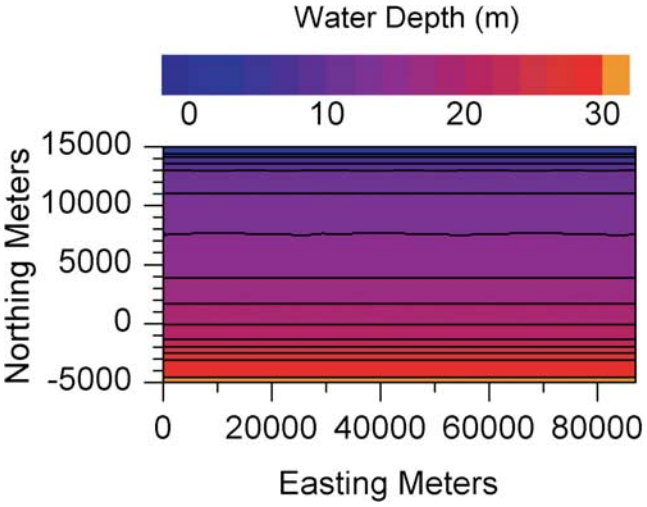

Figure 1. Baseline model bathymetry. The coastline is on the north side of the grid (top of page).

the simple wavefields considered herein. The wave height error analysis and model correction computations are performed on a curvilinear grid (hereinafter called the analysis grid or AG). The analysis grid must be identical to or comprise a subset of the computational grid. In this study, the curvilinear analysis grid is created by using every third row and column from the curvilinear computational grid; thus the number of cells is decreased by a factor of nine, which does not introduce interpolation error but there is a loss of information on the AG. Nodes in this grid are denoted by i_a and j_a along the easting and northing axes, respectively.

[12] The setup for SWAN is the same for all experiments, except for the bottom roughness distribution and bathymetry. The computational grid spans 88 km along the x axis with 176 cells having a uniform spacing of 500 m, and 25 km perpendicular to the coast (y axis) with 43 cells whose dimensions decrease from 1000 m at the seaward margin to 100 m at the coast (Figure 1). The resulting bottom gradient of 1.5×10^{-3} is between that of the U. S. middle-Atlantic shelf (less than 1.1×10^{-2}) and that of the Gulf of Mexico (approximately 6×10^{-4}). The computational grid has a stretched y coordinate because wave damping is insignificant in deeper water and thus high resolution is unnecessary there. A uniform grid with a cell size of 200 m is used for output from SWAN. The open boundary forcing consists of a JONSWAP spectrum applied uniformly on the southern boundary with a peak enhancement factor of 3.3. The mean wave height is 1 m and the wave source direction is oriented 30° from shore normal (coming from south–southeast). There is no smooth and realistic way to specify a lateral boundary condition for this grid orientation in SWAN. The western and eastern boundaries use no wave forcing, which means that the predicted results are invalid for x greater than 60 km (see Figure 1). A directional resolution of 5° is used. Depth-induced breaking is represented in the wave model and would not be a problem if it were included in both the control and inversion runs; however, it is turned off for this study because the spatial resolution of the grid (e.g., grid depths of 0.4 m, 1.4 m, and 2.6 m within the surf zone) is inadequate. The model is used to simulate swell conditions only (no wind input, whitecapping or nonlinear interactions) and thus the computations are stationary. We chose to use three iterations to compute the stationary wavefield using the implicit scheme used by SWAN.

[13] This study focuses on a bottom friction-dominated problem, which is reflected in the included model physics. This simplified model reduces the numerical problem to one with only one dominant physical process, wave damping by bottom friction. Thus the key parameter is well known and problems of parameter identification are minimized. Both refraction and shoaling are included in the model and are expected to be represented accurately. In order to increase the signal-to-noise ratio in the experiments, winds and other coastal forcing fields are not included because they would increase environmental noise that is not explicitly addressed in this study. A background (i.e., regional) bottom roughness is assumed known in order to increase the speed of convergence to solution, but it is not required by the method.

[14] There are two types of geological features used in the simulations, bottom type (friction features) and bathymetry. The friction features, which are on the order of 100 km^2 in area, represent variations in bottom characteristics such as bed forms and sediment type. The spatial scale of sediment heterogeneity varies but mud banks can be as much as 1800 km^2 in extent [*Anthony et al.*, 2002] whereas individual ripples are much smaller. The value of k_b used for these features in the model represents spatial averages of ripple fields. The friction features are simplifications of these bottom types that use only binary friction values (e.g., k_b = 0.07 m or 0.005 m). This simple structure is unknown to the inverse method, which does not utilize information about the parameter distribution in its solution. Therefore the inverse solutions comprise a range of values rather than binary. The bathymetric depressions represent features like drowned river valleys and the elevated areas, which have horizontal dimensions of less than 3000 m, represent shoals and sand ridges [*McBride and Moslow*, 1991].

[15] A total of eight cases are discussed in this report (Table 1). These examples illustrate how well the inversion can recover an unknown bottom roughness distribution. Case (1) is a trivial simulation that has no variations in bottom friction or the bathymetry in Figure 1. It is used to compute the influence matrix as discussed in section 3.1. Cases (2) through (5) examine different k_b distributions (Figure 2) that represent patches of either rougher (k_b = 0.07 m) or smoother (k_b = 0.005 m) bottom on an otherwise uniform seafloor (k_b = 0.05 m). Cases (5) and (6) introduce random noise into the wavefield to determine if the inversion can recover a bottom roughness field that includes a low-friction patch. Case (7) incorporates an unknown embayment that represents a large error in bathymetry, and case (8) includes unknown localized bathymetric highs (amplitude = 0.5–2 m) as well as a patch with reduced bottom roughness.

3. Inversion Method

[16] The inversion described in this paper relies on computing a large number of solutions using a numerical

Table 1. Boundary Conditions and Parameters Used for SWAN Runs

Case	Shelf Gradient and Bathymetry	k_b, m	Wavefield[a]
1[b]	0.0015	0.05	OBC: H_S = 1 m from SSE
2	0.0015	Background = 0.05 m and feature = 0.005 m	OBC: H_S = 1 m from SSE
3	0.0015	Background = 0.05 m and feature = 0.07 m	OBC: H_S = 1 m from SSE
4	0.0015	Background = 0.05 m and two features = 0.07 m	OBC: H_S = 1 m from SSE
5	0.0015	Background 0.05 m and feature = 0.005 m	Case 2 field with random error of ±0.03 m
6	0.0015	Background = 0.05 m and feature = 0.005 m	Case 2 field with random error of ±0.12 m
7	Background = 0.0015 and embayment	0.05 m	OBC: H_S = 1 m from SSE
8	Background = 0.0015 with shoals	Background = 0.05 m and feature = 0.07 m	OBC: H_S = 1 m from SSE

[a]OBC is open boundary condition, and SSE is south southeast.
[b]Case 1 is only used for calculating **IM**.

wave model and finding the optimal solution by minimizing the error in the model-predicted significant wave height. The penalty in terms of slower calculations is considered acceptable because it is possible to improve the numerical technique later to increase efficiency. One advantage is that the procedure is independent of the wave model used. A similar approach was used by *Kennedy et al.* [2000] for determining inverse depths. The algorithm for retrieving the roughness field consists of the following steps.

[17] 1. Collect dense measurements of the wave height field over the area of interest at one time.

[18] 2. Estimate the background bottom roughness field for the region of interest; convergence is faster for an accurate estimate.

[19] 3. Calculate the normalized wave height change relative to Case 1 (the initial, homogeneous estimate of the friction field) on the output grid associated with a small perturbation of the bottom friction at each point on the analysis grid. This matrix, which has a number of columns and rows equal to the number of cells on the OG and AG, respectively, is the Influence Matrix, **IM**.

[20] 4. Run the numerical wave model with the initial bottom friction field (or field updated in step 5) to find the stationary wavefield.

[21] 5. Compare the measured and predicted wave heights and use this result along with **IM** to update the bottom friction field.

[22] 6. If the maximum wave height error is above a specified tolerance, go to step 4; otherwise, end the sequence.

[23] This algorithm contains two key procedures, steps 3 and 5. The Influence Matrix computed in step 3 includes the impact of a change in bottom friction at a given point on every other point within the model grid. It is computed only once using the initial estimate as the friction field. The friction field is updated in step 5 by using the column in **IM** for the cell on the OG with the largest error. Steps 4 through 6 comprise the analysis cycle. The number of analysis cycles required is different for each of the cases discussed in this paper.

3.1. Influence Matrix Calculation

[24] The Influence Matrix, which is calculated in step 3 of the inversion algorithm, contains $no \times mo$ columns and $na \times ma$ rows, where no and mo are the number of cells along the x and y axes on the output grid and na and ma are the axes dimensions of the analysis grid. Each point (i_o, j_o) on the OG corresponds to a column n in **IM**, where $n = 1 \ldots no \times mo$, and every point (i_a, j_a) on the AG corresponds to a row m in **IM**, where $m = 1 \ldots na \times ma$. The elements of **IM** are then found by repeating the following steps for each point on the AG, or row m in **IM**.

[25] 1. The bottom roughness length at cell (i_a, j_a) corresponding to row m is modified from the initial estimate by multiplying by a factor, γk_b. The value of γ should be sufficient to have a noticeable effect (or influence) on the wave height field. We use $\gamma = 0.1$ on the basis of a number of test cases.

[26] 2. A new wavefield is computed with the numerical wave model using the modified friction field.

[27] 3. The normalized change in the predicted wave height $H_{P,n}$ on the output grid (or column n in **IM**) caused by the modified k_b at cell (i_a, j_a) is then given by

$$E_{m,n} = \frac{|H_{1,n} - H_{P,n}|}{E_{\mathrm{MAX}}} \quad n = 1, no \times mo \tag{4}$$

where: $H_{1,n}$ = the wave height predicted by Case 1 (Figure 3a) for each cell on the OG and E_{MAX} = maximum value of E. The normalized change ranges from 0 to 1. Note that E is positive because it represents the strength of the influence only.

[28] After completing these three steps for all rows ($m = 1 \ldots na \times ma$), which correspond to the points on the analysis grid, all of the elements in **IM** have been calculated:

$$\mathbf{IM} = \begin{bmatrix} E_{1,1} & E_{1,2} & E_{1,3} & \ldots & E_{1,no\times mo} \\ E_{2,1} & E_{2,2} & E_{2,3} & \ldots & E_{2,no\times mo} \\ E_{3,1} & E_{3,2} & E_{3,3} & \ldots & E_{3,no\times mo} \\ & & \ldots & & \\ E_{na\times ma,1} & E_{na\times ma,2} & E_{na\times ma,3} & \ldots & E_{na\times ma,no\times mo} \end{bmatrix} \tag{5}$$

[29] The wavefields computed by the numerical model are dependent on the boundary conditions and bathymetry; therefore it is unnecessary to recompute **IM** unless these are intentionally changed. For application to the coastal ocean, **IM** would be calculated for a steady wavefield using available bathymetry but it would need to be recomputed if the wavefield changed during the study interval. The numerical wave model is run $na \times ma$ times (826 for the AG used in this study); of course, these are stationary wavefields, which greatly reduces the computations required.

[30] Each row of **IM** contains the normalized wave height changes on the output grid from (4) for the specified

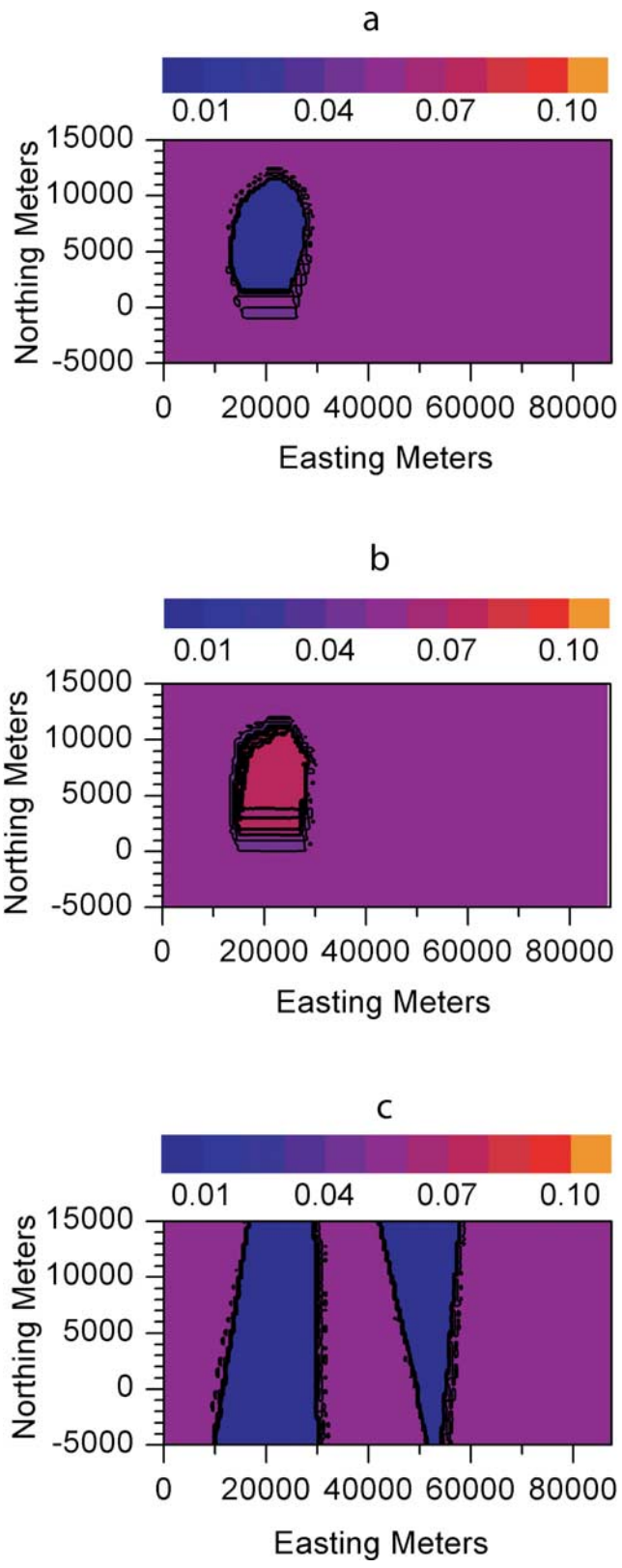

Figure 2. The friction coefficients k_b used for wave simulations. (a) Case 2, feature k_b = 0.005 m, (b) Case 3, feature k_b = 0.07 m, and (c) Case 4, both features have k_b = 0.005 m. The background k_b = 0.05 m. The coastline is on the north side of the grid (top of page).

bottom friction change at a single point on the analysis grid. The choice of the analysis and output grids is not important to the inversion method itself. The grid attributes are selected for convenience of computation and the desired accuracy. We have retained the multiple grid nomenclature for generality. The ordering of grid points in **IM** is not important because the normalized changes E are mutually independent.

3.2. Updating the Friction Field

[31] After a new wavefield has been computed in step 4 of the analysis cycle, the wave heights are compared to the observations (control runs in these examples) in order to modify the bottom roughness length. This step (step 5 of the inversion) is accomplished using the following procedure, which is repeated until the maximum wave height error is within a specified tolerance.

[32] 1. The wave height error at each point on the OG is given by

$$E_{HO} = H_{Ac} - H_c \tag{6}$$

where: H_c is the significant wave height from the control run (c = 2 through 8; see Table 1); and H_{Ac} is the wave height computed by the wave model with the retrieved k_b field. The initial estimate of k_b is used on the first iteration. Note that positive values indicate overprediction. The sign of the error is mapped to the AG and saved as ψ for use in step 3 below.

[33] 2. Noise is removed from the E_{HO} field with a 3 × 3 (2-D nine-point) filter, and the cell with the maximum wave height error magnitude (i_{oe}, j_{oe}), which corresponds to column n_e in **IM**, is found.

[34] 3. Noting that every point (i_a, j_a) on AG corresponds to a row m in **IM**, the roughness length for all grid points on the AG is updated from the previous analysis cycle by

$$k_{b,m}^{p} = k_{b,m}^{p-1} + \Delta k_{b,m}^{p} \qquad m = 1, na \times ma \tag{7}$$

where: p = iteration or analysis cycle; and $\Delta k_{b,m}^{p}$ = change in roughness length, which is given by

$$\Delta k_{b,m}^{p} = \alpha \cdot \mathbf{IM}_{m,n_e} \cdot \boldsymbol{\Psi}_m \quad m = 1, na \times ma \tag{8}$$

where α is a constant with the same units (meters) as the key parameter being retrieved. A larger value of α means more modification to the friction field with each analysis cycle. The sign of the change is obtained from ψ.

[35] Here we assume a linear relationship between the changes in bottom friction and wave height. Faster convergence might be achieved through the use of a more accurate nonlinear relation, particularly when coupled to a relaxation scheme. The constant α was evaluated in a sensitivity study on Case 4 with three parameterizations: (a) a constant value of 0.01 m; (b) using a decreasing step function; and (c) decreasing magnitude with cycle number. The maximum error E_{HO} was reduced to 0.05 m in 680 cycles for a constant value and in fewer than 500 cycles for (c), which had the fastest convergence. A constant value of 0.01 m is used in this paper in order to avoid changing the parameterization for different cases. The most important factor in

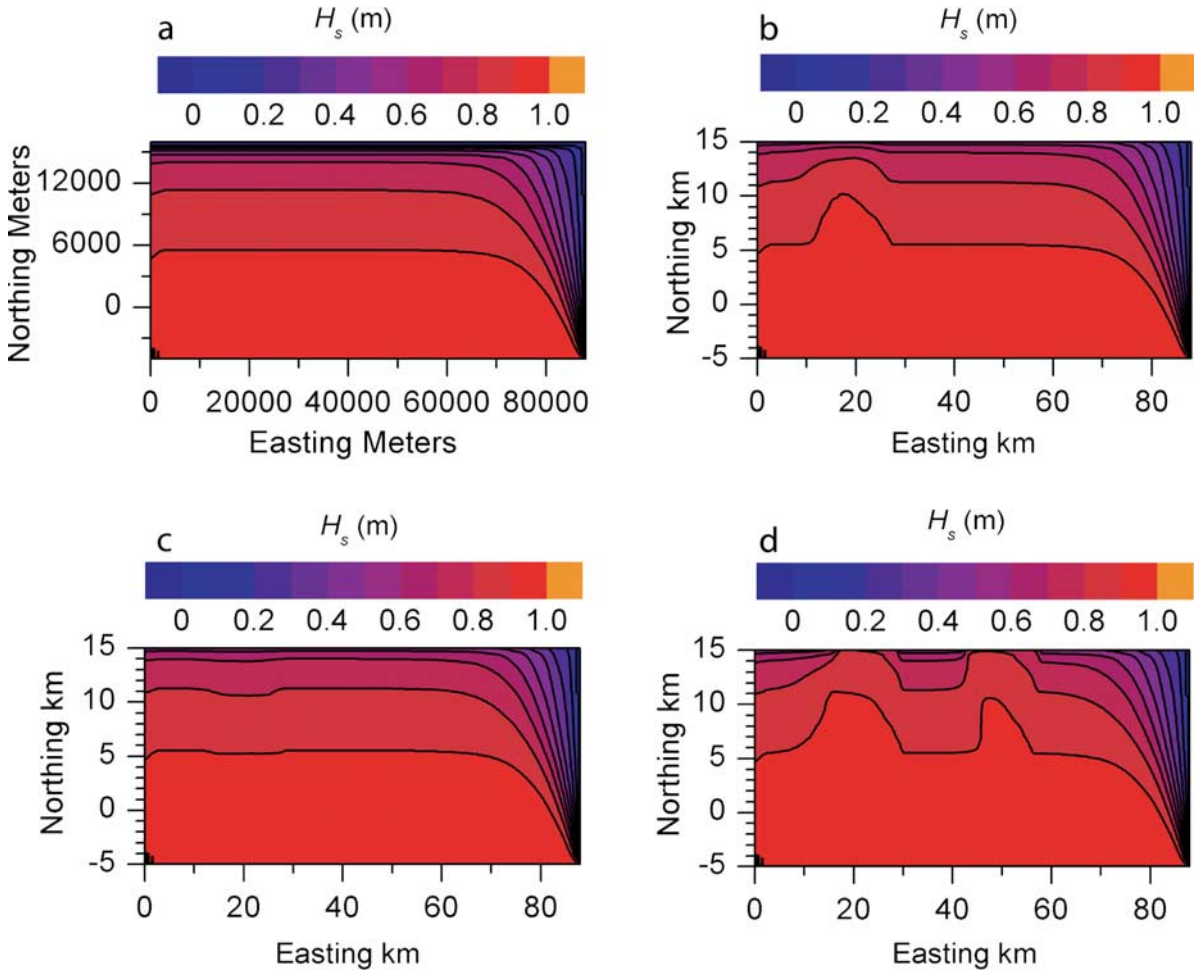

Figure 3. The wave height from the control runs (synthetic observations). (a) Case 1, homogeneous bottom friction used only to calculate **IM**, (b) Case 2, a single feature with decreased bottom friction, (c) Case 3, A single feature with increased bottom friction, and (d) Case 4, two features with decreased bottom friction. The coastline is on the north side of the grid (top of page).

finding the change in bottom roughness from (8) is the value of elements (m, n_e) in **IM** for ($m = 1$, $na \times ma$). This factor reflects the physical influence of bottom friction, as represented by the wave model at cell (i_{oe}, j_{oe}), on all other cells within the physical domain.

4. Inversion Results

[36] This section presents the results of applying the inversion method described above to the cases listed in Table 1. We will refer to simulations using known friction fields as control runs, which serve as proxies for the dense data sets that would ideally be available from remote sensing. We present results for Cases 2 through 8 because Case 1 is only used for computing **IM**. The convergence behavior of the algorithm is evaluated by comparing the significant wave heights computed during the analysis to those from the control run (synthetic observations). The predicted wave heights are very sensitive to errors in bottom roughness and even small errors can indicate problems, requiring examination of the retrieved roughness fields. The accuracy of the solutions will be examined by comparing the retrieved k_b fields to the known fields from the control runs.

4.1. Waves Over an Elliptical Low-Friction Area

[37] The bottom roughness field for Case 2 (Figure 2a) consists of a uniform friction field with $k_b = 0.05$ m, which represents ripples that are 0.05 m high, and an elliptical feature with reduced bottom dissipation ($k_b = 0.005$ m) that extends from a water depth of 12 m to a depth of 20 m. In the ocean a feature like this could be due to finer sediments, which would have smaller ripples. The inversion for this case is presented in detail.

[38] The control run wave heights (Figure 3b) decrease landward away from the feature because the increase in H_S by shoaling is negated by bottom friction. This cross-shore distribution is consistent with observations from a natural beach with similar incident waves [*Elgar et al.*, 1997]. The decreased dissipation over the feature results in higher waves closer to the coast.

[39] A plot of E_{HO} (equation (6)) after one analysis cycle (Figure 4a) shows that the maximum occurs at the shallow end of the feature. The errors are negative over the feature

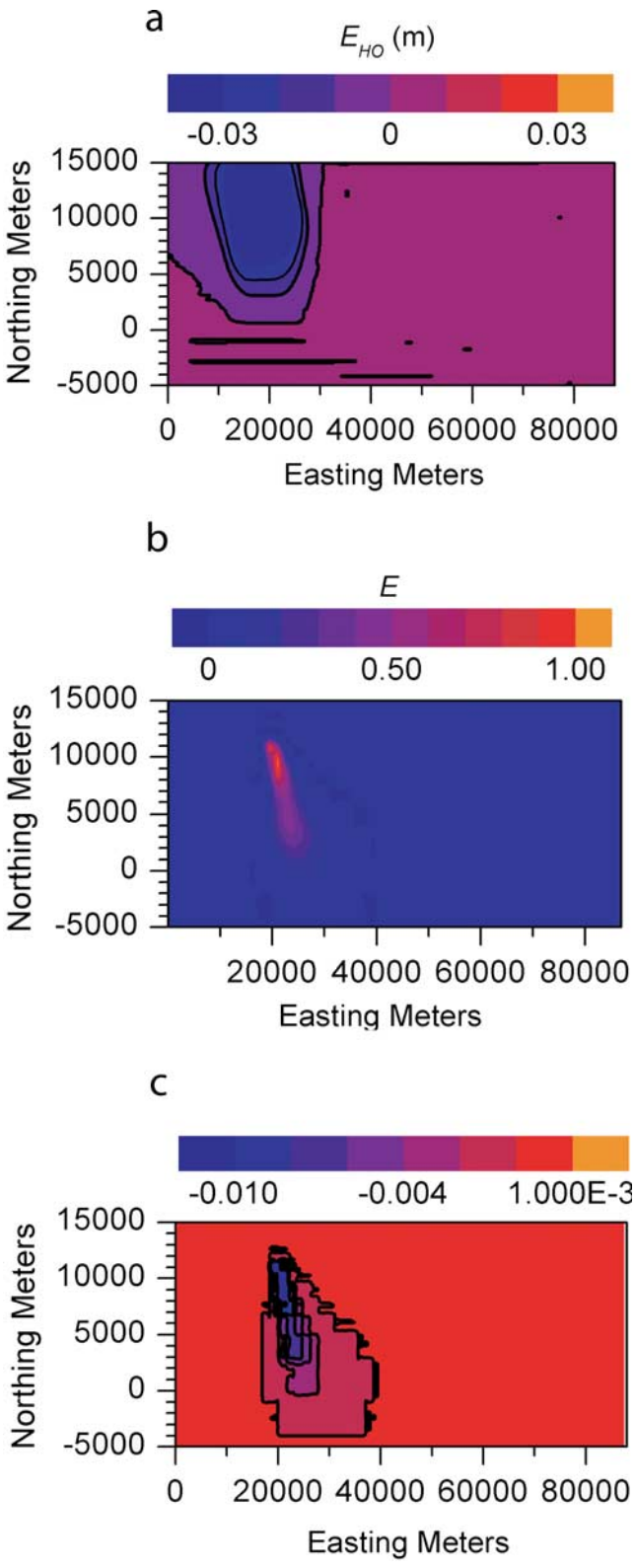

Figure 4. Case 2 results after one analysis cycle. (a) Filtered wave height error E_{HO}, (b) normalized changes E from **IM** corresponding to the point (i_{oe}, j_{oe}), and (c) the change to the friction field Δk_b. The coastline is on the north side of the grid (top of page).

itself because of its much lower roughness (0.005 m) and resulting higher waves in the control run. The values of E found from (4) for column n_e of **IM** (Figure 4b) indicate where a change in bottom friction will have the greatest influence on the wave height at (i_{oe}, j_{oe}). For example, E is near zero far from the friction feature and in deep water, and large at the shallow end of the feature. The largest values of E are oriented south-southeast because bottom dissipation impacts the wavefield on the leeward side of a friction feature. The normalized wave height changes in Figure 4b are used in (8) to calculate the adjustment of the friction field Δk_b after the first analysis cycle (Figure 4c). The largest modifications occur over the center of the feature.

[40] The maximum E_{HO} (Figure 5) decreases to less than 0.01 m (approximately 1% for the 1 m waves used in this study) after fewer than 50 analysis cycles but the inversion continues until the error is below a specified tolerance. The inversion stops after 261 cycles with a calculated significant wave height field (Figure 6a) that is indistinguishable from the control run (Figure 3b) and the values of E_{HO} are near zero (Figure 6b), indicating that the inversion has converged.

[41] The recovered k_b field (Figure 6c) is close to the original (Figure 2a), but the values range from a minimum of 0.005 m to the background value (0.05 m) whereas the control run values have a binary distribution (either 0.005 m or 0.05 m). The normalized mean error between these values and the original field is −4% (k_b overpredicted) and the standard deviation is 45%. Note that the retrieved bottom roughness is less accurate in deeper water.

4.2. Waves Over an Elliptical High-Friction Area

[42] The friction feature for Case 3 (Figure 2b) is similar in plan to Case 2 but k_b is increased to 0.07 m. A larger value of k_b cannot be used because the friction term in SWAN effectively limits the bottom roughness length. The effect of this feature on the wave height (Figure 3c) is weak but noticeable.

[43] The maximum wave height error (Figure 7) decreases from approximately 0.02 m after one cycle to less than 0.0006 m after 41 cycles. The error is positive because the initial estimate for k_b (0.05 m) causes overprediction of the wave heights over the patch. The dependence of the maximum E_{HO} on cycle number is similar to Case 2 (Figure 5) but the solution converges much faster because of the reduced effect of k_b = 0.07 m. This result can be seen by comparing the analysis wave heights (Figure 8a) to the control run (Figure 3c).

[44] The final bottom roughness field (Figure 8b) is similar to the initial field shown in Figure 2b. The mean error for the retrieved k_b field is less than −1% and the standard deviation of the error is less than 4.8%. This result is consistent with the small errors in the predicted wave heights.

4.3. Waves Over Two Cross-Shore Low-Friction Areas

[45] There are two low-friction (k_b = 0.005 m), shore normal features in Case 4 (Figure 2c). This pattern is more representative of a typical inner shelf and shoreface than the previous cases but it also increases the difficulty of the solution. This bottom roughness field has the greatest effect on the control run wave heights (Figure 3d) of the three

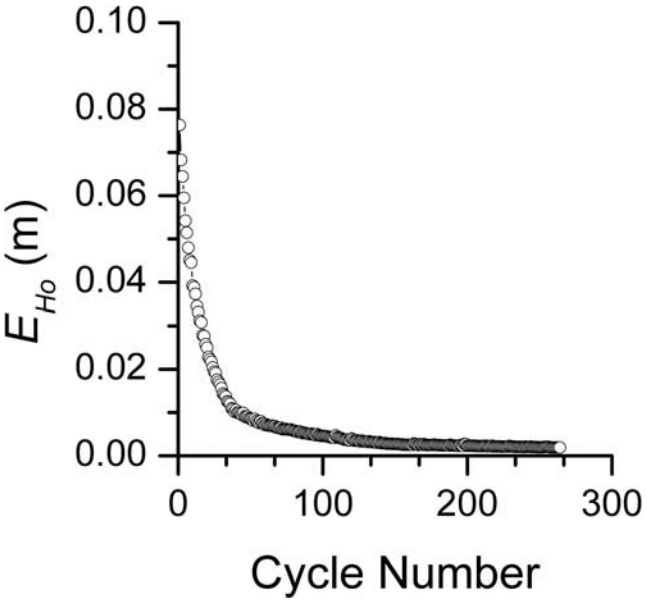

Figure 5. Case 2: the maximum value of the filtered wave height error E_{HO}, as a function of analysis cycle.

cases discussed so far. Wave heights increase at two points along the shore because of the features; however, neither the features nor the wavefield are symmetric.

[46] The maximum E_{HO} after one cycle is 0.3 m (Figure 9), which is much greater than for the previous cases. The maximum occurs within the western feature. The values of E from **IM** corresponding to cell (i_{oe}, j_{oe}) (not shown) indicate that correlation distances are much shorter for these shoreline-attached features than for offshore features. This is consistent with the physical problem; in shallower water, the ratio between near-field wave energy dissipation and far-field dissipation becomes larger; thus the changes in bottom friction that are used in computing **IM** do not have a far-reaching influence.

[47] The maximum E_{HO} decreases to less than 0.03 m after 800 cycles but the inversion continues until cycle 1000. The largest errors (Figure 10a) are in shallow water east of the features. Positive values of E_{HO} result from overcorrection of k_b where no differences in bottom friction actually existed. This is caused by the choice of the AG, which spreads the correction from **IM** over more cells on the OG. The large error (~3%) suggests that the retrieved k_b field should be examined in detail.

[48] The retrieved friction field (Figure 10b) resolves the two features but their shapes have not been fully recovered offshore because the values of E contained in **IM** are relatively small in deeper water. The mean normalized error for k_b is −59% and the standard deviation is 183%. This result suggests that even small errors in wave height can indicate a problem. Furthermore, the mean error is biased by the solution for water depths greater than 15 m, where bottom friction has minimal effect on the incident waves. This problem demonstrates the limitations of using measured wave heights to infer bottom friction coefficients in deep water where wave heights are insensitive to bottom friction. The maximum wave height error does not decrease

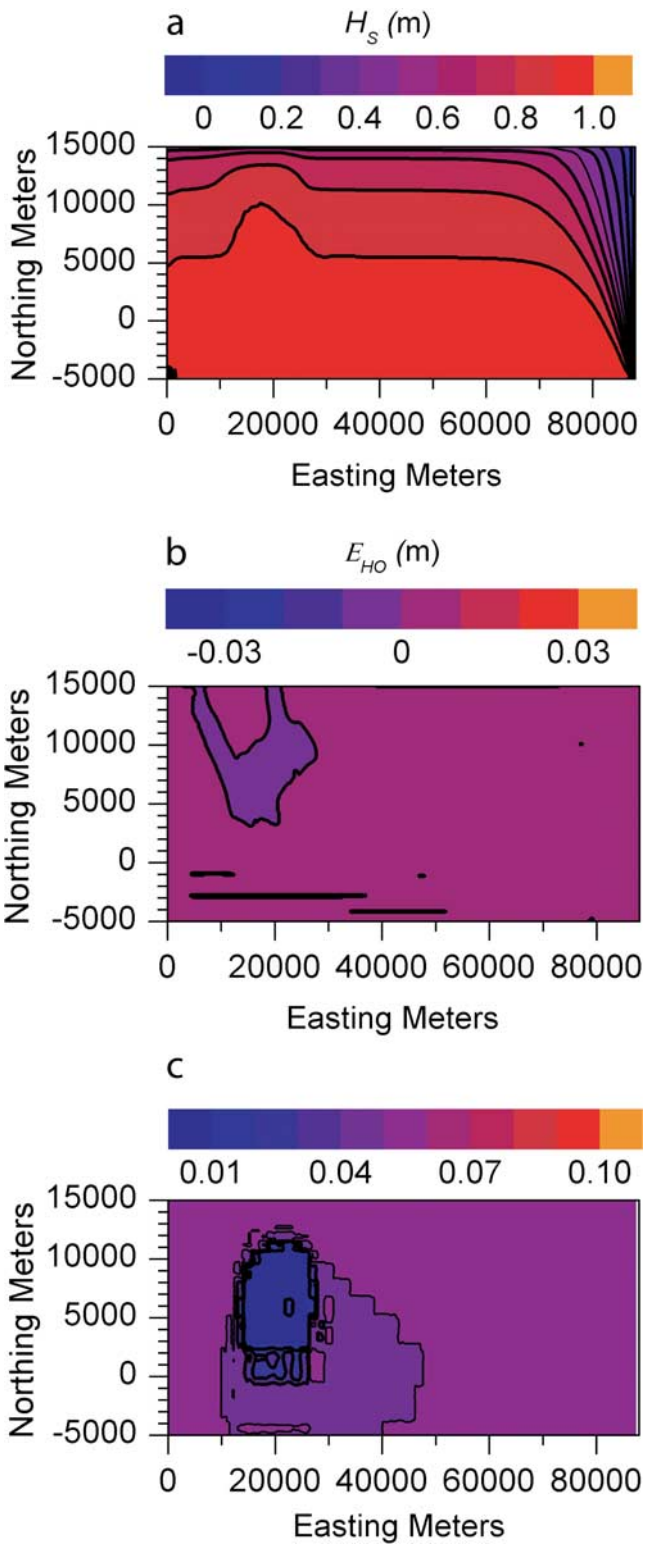

Figure 6. Case 2: results from the inversion analysis at cycle 261. (a) The analysis wave height field, (b) plot of the filtered wave height error E_{HO}, and (c) contour plot of k_b values. The coastline is on the north side of the grid (top of page).

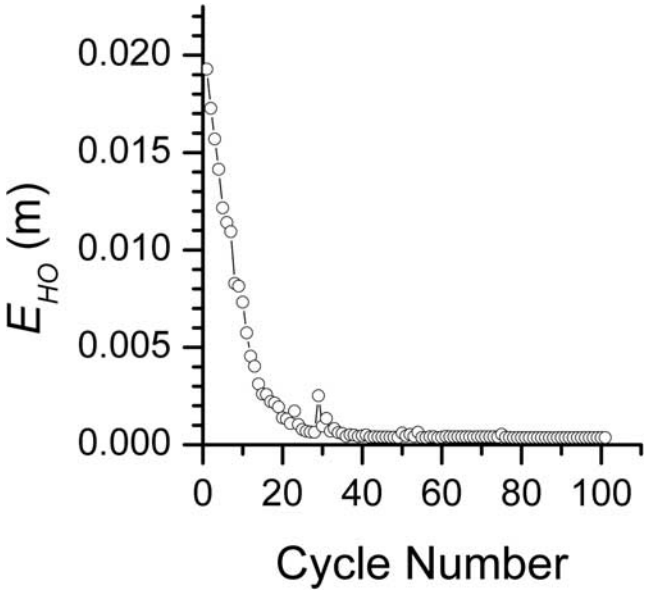

Figure 7. Case 3: the maximum value of the filtered wave height error E_{HO}, as a function of analysis cycle.

below 0.02 m, which is an order of magnitude greater than for the previous runs. It is thus important to note that values of E_{HO} greater than 1% are an indication of poor convergence of the inversion, and an accompanying uncertainty in the retrieved bottom friction field. Nevertheless, the recovered k_b field (Figure 10b) is reasonable for depths shallower than 15 m.

5. Inversion Sensitivity and Uniqueness

[49] The tests discussed in this section use the same boundary condition as in Cases 1 through 6 and *assume* the same bathymetry; therefore **IM** does not need to be recalculated. We will thus evaluate the impact of uncertainty in the measured wavefield (Cases 5 and 6) and examine the inversion result for bottom friction when another key parameter may be poorly known; specifically, bathymetry (Cases 7 and 8).

5.1. Measured Wave Height Uncertainty

[50] Case 5 investigates the effect of uncertainty in the wave measurements by adding random noise to the control run wavefield. When random noise with a standard deviation of 0.03 m (3% of wave height at the open boundary) is added to the wave heights from Case 2, the inversion terminates in 53 cycles with a maximum filtered wave height error of less than 0.015 m, a mean error of −10% for k_b, and a standard deviation of 69%. It is also instructive to find at what level of uncertainty the inversion fails. The inversion stops after 14 iterations when random noise with a standard deviation of 12% is added to the wave height field (Case 6). The value of E in **IM** is zero for column n_e and the inversion stops because it cannot reduce the error at this point further via modification of the friction field. The mean and standard deviation of the k_b error for the entire domain are −26% and 129%, respectively. These errors are larger than for Case 2, which has no noise in the wavefield, but they remain less than for Case 4.

5.2. Bathymetry Uncertainty

[51] It is important to examine the uniqueness of the inversion method with respect to uncertainty in nearshore bathymetry because water depth is a key parameter for the wave model. The purpose of this test is to see if the uncertainty in water depth is erroneously retrieved by the inversion; that is, will the inversion incorrectly identify a bathymetric feature as a low-friction area?

[52] The grid for Case 7 incorporates an embayment with a mean depth of 5 m (Figure 11a) and has a uniform bottom roughness field (k_b = 0.05 m). The inversion assumes that the depression is unknown. Such large bathymetry errors are unlikely but this problem will test the robustness of the inversion algorithm for large errors in more than one key parameter. The predicted wave heights over the feature are similar to those further offshore (Figure 11b) because the incident waves have propagated further before encountering shallow water where dissipation by bottom friction is substantial.

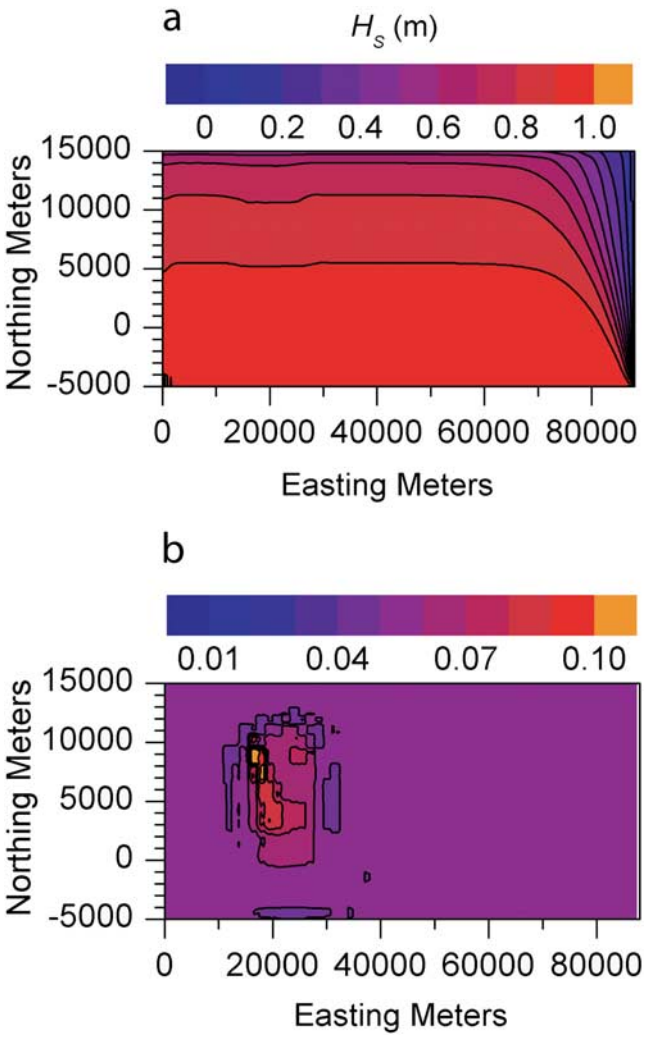

Figure 8. Case 3: final results. (a) The analysis wave height field after 41 cycles and (b) contour plot of k_b values. The coastline is on the north side of the grid (top of page).

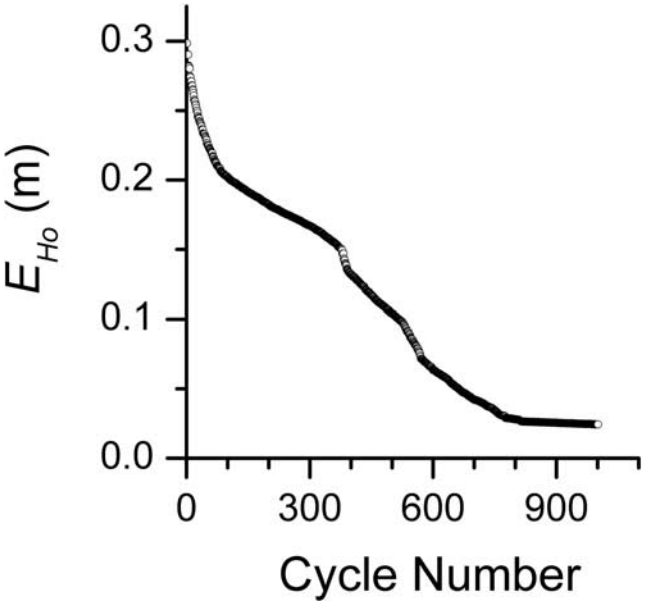

Figure 9. Case 4: plot of the maximum value of the filtered wave height error as a function of analysis cycle.

[53] The inversion terminates after 343 cycles with an error of almost 0.02 m in H_S because the maximum wave height error occurs at a location (i_{oe}, j_{oe}) that is not sensitive to changes in the friction field. Application of **IM** is therefore not possible because all values for column n_e are zero. The maximum error of 0.02 m suggests that the observed variation from the control wavefield is not caused by bottom friction only, and thus the retrieved values of k_b should be examined.

[54] As with Case 3, the greatest modification of the background k_b is in the shallowest water. In fact, the retrieved bottom roughness field (Figure 11c) mirrors the embayment, replacing water depth with smaller values of k_b. The errors increase as the coast is approached and a minimum k_b of 0.005 is retrieved. This example demonstrates why a fundamental assumption of the inversion method is that the bathymetry is known.

[55] We can further examine the inversion's sensitivity to bathymetry errors with a more realistic example. Case 8 uses a high-friction feature (Figure 12a) with k_b = 0.07 m superimposed on a uniform background roughness of 0.02 m. The bathymetry includes multiple shoals, with amplitudes of 0.5–2 m in water depths ranging from 8 to 28 m, superimposed on the smooth bathymetry used in cases (1) through (6) (Figure 12b). The wavefield for the control run (Figure 13a) has lower wave heights over the friction feature because of increased dissipation by bottom friction. The waves are higher, however, over the shoals because of shoaling effects. This can be seen by comparison of the bathymetry in Figure 12b and the wavefield (Figure 13a) along the western end of the grid at y = 7000 m.

[56] The predicted wave heights after 31 analysis cycles (Figure 13b) reflect the influence of the friction feature only, however, and not the shoals. The largest values of E_{HO} (Figure 13c) occur in shallow water over the feature and not where the bathymetry errors are located. On the basis of our previous results, this large error suggests that the inversion is contaminated by another key parameter besides bottom friction (i.e., bathymetry).

[57] The mean and standard deviation for the k_b errors are less than −1% and 15%, respectively, and comparing the retrieved bottom roughness field (Figure 13d) to the original field (Figure 12a) shows that the largest k_b error occurs in shallow water and is not associated with the unknown shoals. This example demonstrates the importance of examining the distributions rather than relying on overall statistical parameters, which include errors in deep water as well as shallow. Given this precaution, it appears that the inversion recovers the unknown friction feature reasonably well (low-k_b error) while indicating that there are other important features within the region that affect wave height (high E_{HO}). However, as suggested by case 4, whenever the wave height error is more than 1% it is necessary to examine the retrieved bottom roughness field to see if it is physically realistic.

6. Discussion and Conclusions

[58] These results suggest that the approach works well for friction-dominated areas where swell is the main source

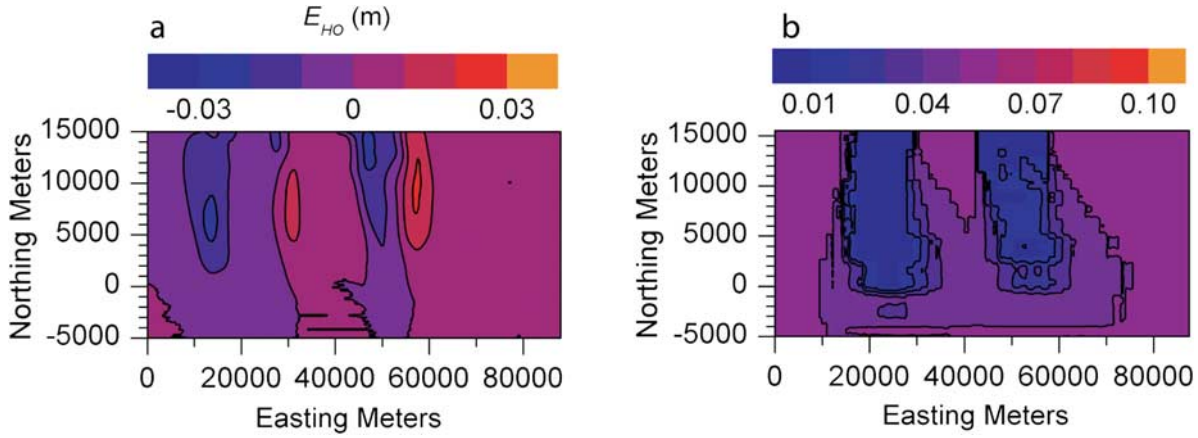

Figure 10. Case 4: results after 1000 analysis cycles. (a) Plot of the filtered wave height error E_{HO} and (b) contour plot of k_b values. The coastline is on the north side of the grid (top of page).

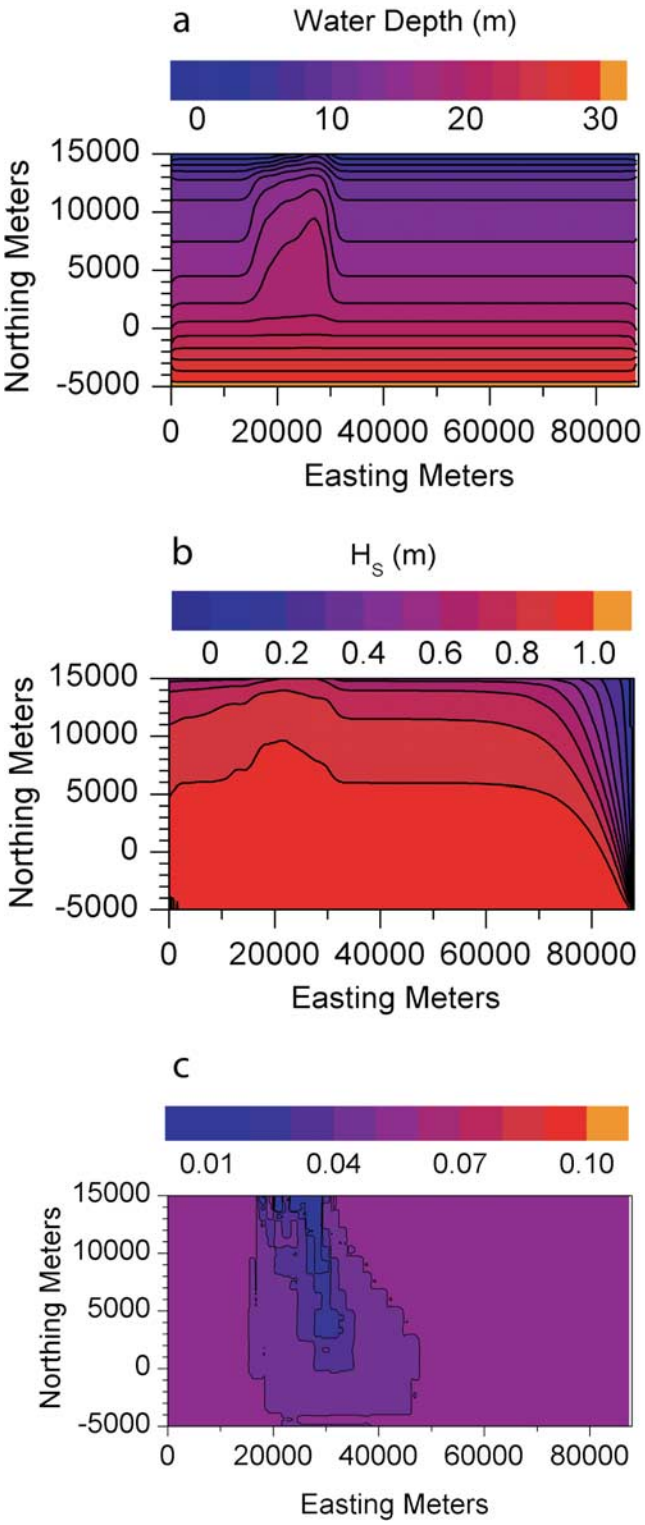

Figure 11. Case 7: results after 31 cycles. (a) Bathymetry, (b) predicted values of significant wave height, and (c) contour plot of k_b values. The coastline is on the north side of the grid (top of page).

of waves, but there are several constraints that must be considered in applying it to realistic problems. Field data of sufficient density to validate the inversion were not available for use in this study and it was necessary to use synthetic observations, which also reduced the uncertainty of the results. As demonstrated by the results for random noise (Cases 5 and 6), small measurement errors slow convergence but do not render the inversion inaccurate. Synthetic Aperture Radar (SAR) data can be processed to retrieve wave heights but errors can be as much as 29% [*Mastenbroek and de Valk*, 2000]. Shore-based radar systems [e.g., *Gurgel et al.*, 1999] could also be useful for providing wave measurements analogous to the synthetic measurements used in this study. These approaches have problems but their continued development suggests that dense wave height observations with errors less than 10% are not an unreasonable expectation in the future.

[59] This study uses a small computation domain in order to facilitate development and testing of the inversion algorithm. If a larger grid had been used for the SWAN simulations, it would have been difficult to develop the algorithm described in this paper, which was intended for use on desktop computers. This is a common difficulty with inverse solutions and data assimilation. There is no inherent problem with scaling the method to larger or more complex problems. It should be noted, however, that the domain size used in this study is appropriate for problems of nearshore dynamics [e.g., *Keen et al.*, 2003].

[60] A critical element of the inversion method discussed in this paper is the Influence Matrix, **IM**, which reflects the impact of wave propagation throughout the domain as represented by the physics of the wave model. Thus the values of E display ellipses with their major axes aligned in the direction of wave propagation for the friction-dominated dissipation in this study. For a bathymetry inversion, however, we would expect E to be more concentrated because of the local effect of water depth on wave height through shoaling. Inversions of the type discussed in this paper should work therefore as long as the key parameters produce unique Influence Matrices. It is possible to recalculate **IM** during the inversion procedure in order to reduce the maximum wave height error further but this has not been investigated yet.

[61] Equation (8) contains a dimensional constant α that must be chosen on the basis of the magnitude of the key parameter being retrieved. A series of sensitivity analyses on the value of α were completed, and it was varied over an order of magnitude. The results of these tests indicate that the magnitude of α has a significant effect on the speed of convergence but only a minor impact on the final solution, with a speed up of 28% between a constant of 0.01 m and a variable magnitude. A larger value means more modification to the friction field with each analysis cycle, which is good for the first few cycles. Thus we can incorporate a lack of knowledge of the correlation between grid points into its magnitude; for example, if we are uncertain of the influence of distant effects we would want to use a smaller value.

[62] The inversion method described in this paper is similar to traditional data assimilation approaches but there are important differences. For example, this work is focused on the need to learn more about bottom type rather than improve wave forecasting [*Sheremet and Stone*, 2003]. This

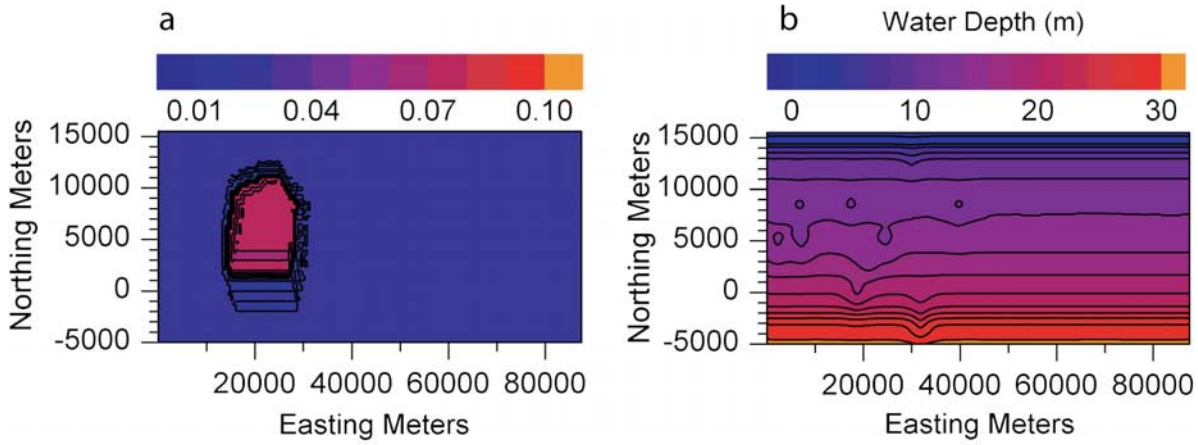

Figure 12. Case 8: friction feature and bathymetry. (a) Contour plot of k_b values and (b) bathymetry. The coastline is on the north side of the grid (top of page).

is a difficult research subject because of the problem of measuring bottom friction parameters in the ocean. Inverse methods that focus on key parameters are important to identify fundamental relationships between measurable wave properties and bottom characteristics. Another important consideration in developing an approach to study this problem is the commitment to development of an adjoint model. Examining basic cause-and-effect relationships does not require such an extensive approach and may even be better served by occasionally using different wave models.

[63] This paper includes a description of the inversion method and presents the results of some simple tests that are

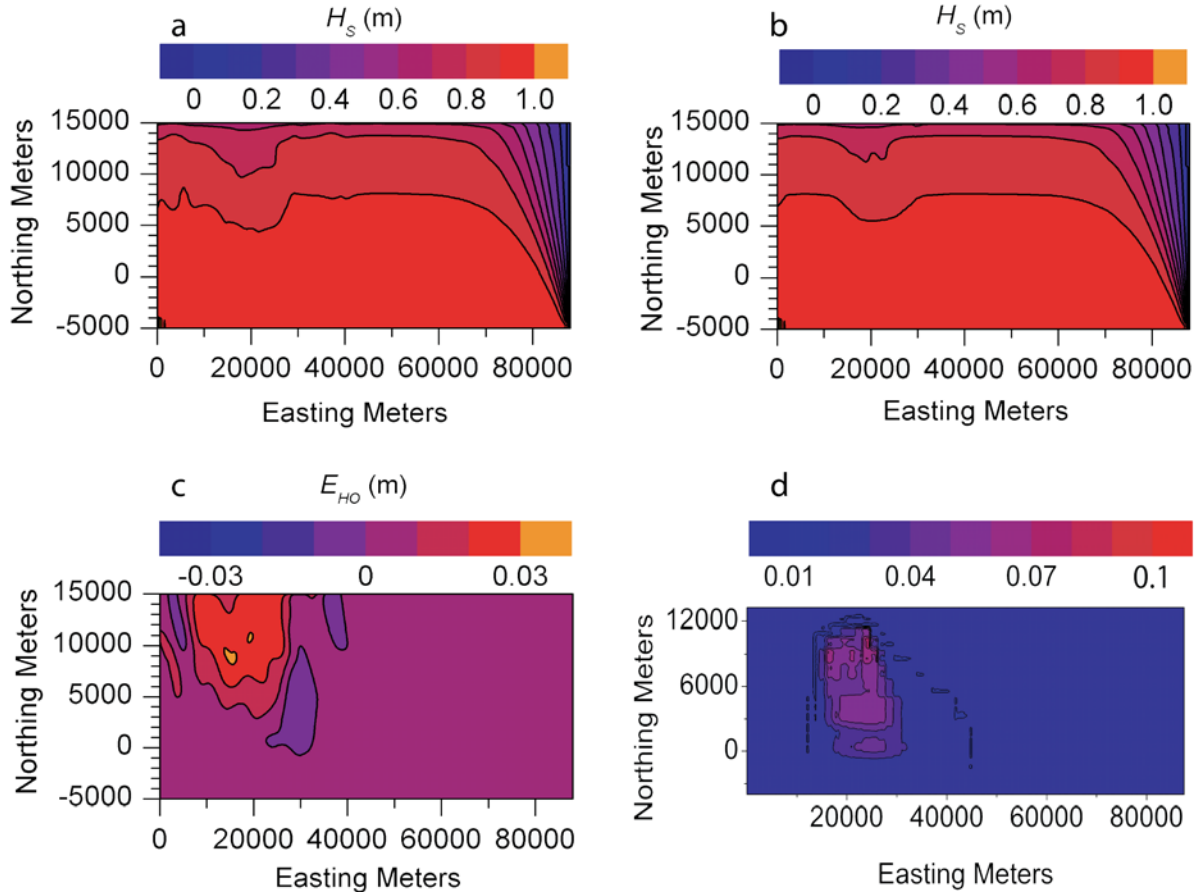

Figure 13. Case 8: results. (a) Predicted wave heights for the control run, (b) the final analysis wave heights (c) contour plot of final E_{HO}, and (d) contour plot of final k_b values. The coastline is on the north side of the grid (top of page).

intended to demonstrate its usefulness in friction-dominated inner shelf areas. In addition, the analysis of measurement error indicates that it is robust and will work with real observations. However, the inversion incorrectly adjusts the bottom roughness length when the bathymetry is poorly known. This effect is less for random uncertainty than systematic errors like the embayment examined in Case 7. This is an important point because water depth is another key parameter for numerical wave models. This highlights the need to identify the key parameters in the model and evaluate their sensitivity before applying this kind of approach. The ability to isolate bottom friction errors from water depth errors is crucial to evaluate bottom sediment type using wave observations, but it may be possible to perform joint inversions for bottom friction and bathymetry [*Holland*, 2001]. The inversion presented in this paper says nothing about the unresolved errors caused by other factors but it seems reasonable to speculate that a similar procedure could be applied to bathymetric errors as well. The usefulness of the algorithm relies on the treatment of applicable physical processes in the numerical wave model.

[64] This approach has limitations that restrict its applicability to scientific problems rather than improving wave forecasts. If the predicted wave height errors are small (<1%), it is probable that bottom friction is the dominant process but in the presence of other important sources of error like bathymetry, it is necessary to examine the results for physical realism. Nevertheless, it can be a useful research tool that, if used properly, can help identify regions of likely high dissipation (e.g., cohesive sediment) even where uncertainty exists in the water depth.

[65] **Acknowledgments.** This work was supported by the Office of Naval Research through the NRL Core project, "Coastal Dynamics in Heterogeneous Sedimentary Environments," (program element 61153N). The comments and encouragement of Nathaniel Plant are gratefully acknowledged. This manuscript has been significantly improved by the comments of the anonymous reviewers.

References

Anderson, D. L. T., J. Sheinbaum, and K. Haines (1996), Data assimilation in ocean models, *Rep. Prog. Phys.*, *59*, 1209–1266.

Anthony, E. J., A. Gardel, F. Dolique, and D. Guiral (2002), Short-term changes in the plan shape of a sandy beach in response to sheltering by a nearshore mud bank, Cayenne, French Guiana, *Earth Surf. Processes Landforms*, *27*, 857–866.

Ardhuin, F., W. C. O'Reilly, T. H. C. Herbers, and P. F. Jessen (2003), Swell transformation across the continental shelf. Part I: Attenuation and directional broadening, *J. Phys. Oceanogr.*, *33*, 1921–1939.

Beck, M. B. (1987), Water-quality modeling: A review of the analysis of uncertainty, *Water Resour. Res.*, *23*, 1393–1442.

Bennett, A. F. (1992), *Inverse Methods in Physical Oceanography*, 346 pp., Cambridge Univ. Press, Cambridge.

Bertino, L., G. Evensen, and H. Wackernagel (2003), Sequential data assimilation techniques in oceanography, *Int. Stat. Rev.*, *71*, 223–241.

Bidlot, J. R., and M. W. Holt (1999), Numerical wave modeling at operational weather centres, *Coastal Eng.*, *37*, 409–429.

Booij, N., R. C. Ris, and L. H. Holthuijsen (1999), A third-generation wave model for coastal regions: 1. Model description and validation, *J. Geophys. Res.*, *104*, 7649–7666.

Dalrymple, R. A., A. B. Kennedy, J. T. Kirby, and Q. Chen (1998), Determining bathymetry from remotely sensed images, in *Coastal Engineering 1998*, edited by B. Edge, pp. 2395–2408, Am. Soc. of Civ. Eng., Reston, Va.

Elgar, S., R. T. Guza, B. Raubenheimer, T. H. C. Herbers, and E. L. Gallagher (1997), Spectral evolution of shoaling and breaking waves on a barred beach, *J. Geophys. Res.*, *102*, 15,797–15,805.

Feddersen, F., E. L. Gallagher, R. T. Guza, and S. Elgar (2003), The drag coefficient, bottom roughness, and wave-breaking in the nearshore, *Coastal Eng.*, *48*, 189–195.

Greenslade, D. J. M. (2001), The assimilation of ERS-2 significant wave height data in the Australian region, *J. Mar. Syst.*, *28*, 141–160.

Grilli, S. T. (1998), Depth inversion in shallow water based on nonlinear properties of shoaling periodic waves, *J. Coastal Eng.*, *35*, 185–209.

Gurgel, K. W., G. Antonischki, H. H. Essen, and T. Schlick (1999), Wellen Radar (WERA): A new ground-wave HF radar for ocean remote sensing, *Coastal Eng.*, *37*, 219–234.

Haus, B. K. (2007), Surface current effects on the fetch-limited growth of wave energy, *J. Geophys. Res.*, *112*, C03003, doi:10.1029/2006JC003924.

Holland, K. T. (2001), Application of the linear dispersion relation with respect to depth inversion and remotely sensed imagery, *IEEE Trans. Geosci. Remote Sens.*, *39*, 2060–2072.

Holthuijsen, L. H., N. Booij, M. vanEndt, S. Caires, and C. G. Soares (1997), Assimilation of buoy and satellite data in wave forecasts with integral control variables, *J. Mar. Syst.*, *13*, 21–31.

Kaihatu, J. M., and A. Sheremet (2004), Dissipation of wave energy by cohesive sediments, in *Coastal Engineering 2004*, edited by J. M. Smith, pp. 498-507, World Sci., Hackensack, N. J.

Keen, T. R., G. Stone, J. M. Kaihatu, and Y. L. Hsu (2003), Barrier island erosion during a winter cold front in Mississippi Sound, in *Coastal Sediments 2003* [CD-ROM], edited by R. A. Davis, A. H. Sallenger Jr., and P. Howd, 13 pp., World Sci., Hackensack, N. J.

Kennedy, A. B., R. A. Dalrymple, J. T. Kirby, and Q. Chen (2000), Determination of inverse depths using direct Boussinesq modeling, *J. Waterw. Port Coastal Ocean Eng.*, *126*, 206–214.

Le Dimet, F. X., and O. Talagrand (1986), Variational algorithms for analysis and assimilation of meteorological observations: Theoretical aspects, *Tellus, Ser. A*, *38*, 97–110.

Madsen, O. S., Y. K. Poon, and H. C. Graber (1988), Spectral wave attenuation by bottom friction: Theory, in *Coastal Engineering* [*1988*], edited by B. L. Edge, pp. 492–504, Am. Soc. of Civ Eng., Reston, Va.

Mastenbroek, C., and C. F. de Valk (2000), A semiparametric algorithm to retrieve ocean wave spectra from synthetic aperture radar, *J. Geophys. Res.*, *105*, 3497–3516.

McBride, R. A., and T. F. Moslow (1991), Origin, evolution, and distribution of shoreface sand ridges, Atlantic inner shelf, U.S.A., *Mar. Geol.*, *97*, 57–85.

Narayanan, C., V. N. R. Rao, and J. M. Kaihatu (2004), Model parameterization and experimental design issues in nearshore bathymetry inversion, *J. Geophys. Res.*, *109*, C08006, doi:10.1029/2002JC001756.

O'Reilly, W. C., and R. T. Guza (1998), Assimilating coastal wave observations in regional swell predictions. Part I: Inverse methods, *J. Phys. Oceanogr.*, *28*, 679–691.

Sheremet, A., and G. W. Stone (2003), Observations of nearshore wave dissipation over muddy sea beds, *J. Geophys. Res.*, *108*(C11), 3357, doi:10.1029/2003JC001885.

Sun, N. Z., M. Elimelech, and J. N. Ryan (2001), Sensitivity analysis and parameter identifiability for colloid transport in geochemically heterogeneous porous media, *Water Resour. Res.*, *37*, 209–222.

Wackerman, C., D. Lyzenga, E. Ericson, and D. Walker (1998), Estimating near-shore bathymetry using SAR, in *Proceedings of the 1998 International Geoscience and Remote Sensing Symposium—Sensing and Managing the Environment*, edited by T. I. Stein, pp. 1668–1670, Inst. of Electr. and Electr. Eng., New York.

Weisse, R., and F. Feser (2003), Evaluation of a method to reduce uncertainty in wind hindcasts performed with regional atmospheric models, *Coastal Eng.*, *48*, 211–225.

J. Dykes, J. M. Kaihatu, T. R. Keen, and W. E. Rogers, Oceanography Division, Naval Research Laboratory, Stennis Space Center, MS 39529, USA. (keen@nrlssc.navy.mil)

K. T. Holland, Marine Geosciences Division, Naval Research Laboratory, Stennis Space Center, MS 39529, USA.